Journal of Biomechanics 57 (2017) 8–17

Contents lists available at ScienceDirect

Journal of Biomechanics

journal homepage: www.elsevier.com/locate/jbiomech
www.JBiomech.com

A benchtop biorobotic platform for *in vitro* observation of muscle-tendon dynamics with parallel mechanical assistance from an elastic exoskeleton

Benjamin D. Robertson [a,b,*], Siddarth Vadakkeveedu [a], Gregory S. Sawicki [a]

[a] Joint Department of Biomedical Engineering, University of North Carolina-Chapel Hill and North Carolina State University, Raleigh, NC, USA
[b] Department of Bioengineering, Temple University, Philadelphia, PA, USA

ARTICLE INFO

Article history:
Accepted 7 March 2017

Invited submission as American Society of Biomechanics 2016 Journal of Biomechanics Award winner

Keywords:
Biomechanics
Elastic exoskeleton
Muscle-tendon mechanics
Unconstrained work loops
Biorobotics

ABSTRACT

We present a novel biorobotic framework comprised of a biological muscle-tendon unit (MTU) mechanically coupled to a feedback controlled robotic environment simulation that mimics *in vivo* inertial/gravitational loading and mechanical assistance from a parallel elastic exoskeleton. Using this system, we applied select combinations of biological muscle activation (modulated with rate-coded direct neural stimulation) and parallel elastic assistance (applied via closed-loop mechanical environment simulation) hypothesized to mimic human behavior based on previously published modeling studies. These conditions resulted in constant system-level force-length dynamics (*i.e.,* stiffness), reduced biological loads, increased muscle excursion, and constant muscle average positive power output—all consistent with laboratory experiments on intact humans during exoskeleton assisted hopping. Mechanical assistance led to reduced estimated metabolic cost and MTU apparent efficiency, but increased apparent efficiency for the MTU + Exo system as a whole. Findings from this study suggest that the increased natural resonant frequency of the artificially stiffened MTU + Exo system, along with invariant movement frequencies, may underlie observed limits on the benefits of exoskeleton assistance. Our novel approach demonstrates that it is possible to capture the salient features of human locomotion with exoskeleton assistance in an isolated muscle-tendon preparation, and introduces a powerful new tool for detailed, direct examination of how assistive devices affect muscle-level neuromechanics and energetics.

1. Introduction

Due to rapid advances in batteries, actuators, and wearable sensors, the promise of robotic exoskeletons to restore or augment human locomotion is coming to fruition (Ferris, 2009). In recent years, we have seen rapid development of exoskeletons for use within (Caputo and Collins, 2014; Ferris and Lewis, 2009; Hocoma; Malcolm et al., 2013) and beyond (Elliot et al., 2013; Hasegawa and Ogura, 2013; Kawamoto et al., 2003; Mooney et al., 2014; Wehner et al., 2013; Wiggin et al., 2011; Zoss et al., 2006) laboratory/clinical settings. Unfortunately, the physiological benefit to the user has not progressed as rapidly, and there are only a handful of reports demonstrating reduced metabolic energy cost with a wearable locomotion assistance device (Collins et al., 2015; Malcolm et al., 2013; Mooney et al., 2014; Panizzolo et al., 2016).

A major barrier to uncovering how metabolic benefit is derived from an assistive exoskeleton is understanding the influence of external torques on underlying muscle function. Experimental methods that use hopping as a model of bouncing gait in combination with electromyography, ultrasound imaging, and inverse dynamics can give insight into how and why muscle forces change when working in parallel with an exoskeleton (Farris et al., 2013). Unfortunately, these physiological measurements are difficult to make alongside devices designed to be in close contact with the limb, and few studies of exoskeleton assisted locomotion are accompanied by the instrumentation necessary for in depth understanding of alterations in muscle-level function.

Despite these difficulties, a common theme has emerged from studies of exoskeleton assisted hopping: external application of force in parallel with a compliant muscle-tendon unit (MTU) can disrupt 'tuned' muscle-tendon interaction dynamics critical during steady, rhythmic locomotion. Previous studies have observed that humans prefer to keep their joint and limb-level mechanics constant when wearing assistive *or* resistive devices (Chang et al.,

* Corresponding author at: Temple University, Department of Bioengineering, 1947 N 12th Street, Philadelphia, PA 19122, USA.
E-mail address: tuf84240@temple.edu (B.D. Robertson).

http://dx.doi.org/10.1016/j.jbiomech.2017.03.009
0021-9290/

2008; Kao et al., 2010), that assistive devices lead to a reduction in force produced in contractile elements (CE, *i.e.,* active muscle) of the biological MTU (Farris et al., 2013; Farris and Sawicki, 2012), and that the amount of energy that can be stored/returned in series elastic elements (SEE, *e.g.,* tendon, aponeurosis) is reduced (Farris et al., 2013).

The ability to cycle a portion of center of mass energy in elastic tissues has been identified as a mechanism for reducing energetic demands and enhancing efficiency of gait (Roberts and Azizi, 2011). Despite evidence that elastic exoskeletons disrupt 'tuned' muscle-tendon interactions, they can still provide net metabolic benefit for the user (Collins et al., 2015; Farris et al., 2013; Grabowski and Herr, 2009). Interestingly, metabolic benefit does not scale directly with the exoskeleton spring stiffness, and there is compelling evidence that too much assistance (*i.e.* a device that is too stiff) can actually increase metabolic demands beyond levels required for unassisted movement (Farris and Sawicki, 2012; Grabowski and Herr, 2009). Simple models have provided some insight into this phenomenon, and predicted limits on energetic benefits as a function of device stiffness, measurable physiological properties of the limb, and performance goals (Robertson et al., 2014; Robertson and Sawicki, 2014; Sawicki and Khan, 2016).

Simulations of exoskeleton-human interaction based on simple Hill-type muscle models provide meaningful insight, but cannot capture all aspects of muscle force production (*e.g.,* history dependence) (Josephson, 1999) that are relevant when considering submaximal eccentric contractions common in exoskeleton assisted locomotion (Farris et al., 2013). To eliminate reliance on limited muscle models in a simulation framework, we developed a novel benchtop bio-robotic platform to mimic the *in-vivo* mechanical environment of muscle-tendon during cyclic contractions (*i.e.,* hopping) with or without exoskeleton assistance. We also implemented a neural controller based on rate coding that can reliably stimulate biological muscle over a range of activation levels (Stevens, 1996).

Using model predictions (Robertson et al., 2014) and a modified version of the novel biorobotic experimental framework from a previous study (Robertson and Sawicki, 2015), we identified appropriate combinations of muscle activation/exoskeleton stiffness to mimic human behavior during hopping with elastic assistance on the benchtop. We hypothesized that assistance from an elastic exoskeleton would: (**H1**) reduce forces in the biological muscle-tendon unit (MTU); (**H2**) reduced biological forces and tendon strains would result in increased muscle fascicle shortening velocities; and (**H3**) reduced biological forces and increased muscle shortening velocities would result in constant average muscle positive mechanical power output. Finally, we postulated that (**H4**) the combination of these outcomes would ultimately result in a constant system stiffness across both assisted and unassisted conditions.

2. Methods

2.1. Animal subjects and surgical preparation

This study was performed in accordance with protocols approved by the NC State Institutional Animal Care and Use Committee (IACUC). Surgical procedures used here have been previously described in detail (Robertson and Sawicki, 2015). In brief, five adult *Rana Lithobates* bullfrogs were euthanized, a hind limb was removed and the plantaris-Achilles tendon MTU was isolated. The Achilles tendon was freed from its distal insertion point, while the plantaris attachment at the knee was left intact and portions of femur and tibia were used to anchor the MTU to a rigid plexiglass chamber with circulating oxygenated ringers solution at 27 °C. Sonomicrometry crystals (1 mm diameter, Sonometrics Inc., London, Ontario, CA) were implanted along a muscle fascicle, and free tendon was inserted into a friction clamp attached via rigid aircraft cable to a feedback controlled motor (Aurora 310B-LR, Aurora Scientific, Aurora, Ontario, CA). Great care was taken to preserve the sciatic nerve, to which a bipolar stimulating electrode cuff was attached (cuff: Microprobes for Life Science, Gaithersburg, MD, USA, stimulator: Aurora Scientific, Aurora, Ontario, CA).

2.2. Motor controller

The motor controller was a modified version of the one used to simulate an inertial/gravitational load in a previous study (Robertson and Sawicki, 2015). We added a parallel elastic exoskeleton to mechanical environment simulations using the approach outlined in a prior computer simulation study (Robertson et al., 2014) (Fig. 1A). Details of motor controllers and implementation can be found in Supplementary methods.

2.3. Muscle stimulation controller

We used a 'pulsed' rate coding approach to modulate force/activation as described in Stevens (Stevens, 1996). Using an assumed experimental driving frequency (ω_{Drive}) of 2 Hz (discussed in detail below), and a set stimulation duty of 10% of a driving cycle period (*i.e.,* $T_{stim} = 10\%\omega_{Drive}^{-1} = 50$ ms), we performed a small study ($n = 3$) to determine the influence of ω_{spike} on peak force (F_{peak}) output (Fig. 1B). The muscle preparation was the same as those detailed above, except the free tendon was clamped at the muscle tendon junction to minimize shortening against series compliant tissues. The ergometer arm was set to a fixed position for which passive muscle force was ~1 N, and the muscle was subjected 5 experimental conditions consisting of 3 consecutive contractions ($\omega_{Drive} = 2$ Hz, $T_{stim} = 50$ ms) with ω_{spike} values of 20, 40, 60, 80, and 100 Hz (*i.e.,* # spikes/pulse = 1, 2, 3, 4, and 5, respectively). Based on previous research, we assumed that ω_{spike} of 100 Hz resulted in maximal muscle activation (Pennycuick, 1964; Rack and Westbury, 1969; Stevens, 1996). The order of the ω_{spike} conditions was randomized to counteract fatigue effects. Peak forces achieved in each of the 3 contractions were averaged and normalized to the peak force from the 100 Hz condition.

2.4. Environment and exoskeleton parameter selection

We selected motor controller parameters to maintain the same system resonant frequency (ω_0) across conditions and preparations. System resonant frequency was assumed to adhere to the following equation:

$$\omega_0 = \frac{l_{in}}{l_{out}}\sqrt{\frac{k_{MTU}}{M}} \quad (1)$$

where k_{MTU} is effective passive MTU stiffness, M is system mass, and l_{in}/l_{out} are MTU input and mass output moment arms, respectively (Fig. 1A). To initially determine ω_0 and k_{MTU} for each experimental preparation, the MTU was allowed to oscillate passively against a simulated inertial/gravitational load previously used in similar experiments (Robertson and Sawicki, 2015) ($l_{in} = 1, l_{out} = 21, M = 0.085$ kg) (Fig. 1C).

Once k_{MTU} was determined, l_{out} and M were varied to approximate $\omega_0 = 2$ Hz for each preparation (Table 1, Fig. 1C). In subsequent dynamic conditions, simulated exoskeleton spring stiffness was set as a percentage of measured k_{MTU} based on previous modeling results (Robertson et al., 2014). In the aforementioned *in silico* studies, k_{Exo} was scaled as a percentage of modeled SEE stiffness, which was triple the stiffness of the whole MTU (*i.e.,* $k_{SEE} = 3k_{MTU}$). Because we used measured k_{MTU} values as a guide in the current study, model based predictions were adjusted accordingly (*e.g.,* the $k_{Exo} = 60\%k_{MTU}$ condition here is comparable to the $k_{Exo} = 20\%k_{SEE}$ in previous simulation work). (Robertson et al., 2014).

2.5. Experimental execution

A 300 ms fixed end contraction was performed under an initial passive load (~10 N, based on previous experience) to determine an approximate value of peak isometric force (F_{max}) for active muscle. Next, an initial passive pluck was performed, k_{MTU} was determined, and system inertial parameters were adjusted to approximate $\omega_0 \sim 2$ Hz. Then, 3 consecutive fixed end contractions ($\omega_{Drive} = 2.0$ Hz, $T_{stim} = 50$ ms, $\omega_{spike} = 100$ Hz) were performed to determine a baseline average peak force for a later fatigue assessment.

Following initial identification of system parameters, five combinations of normalized exoskeleton stiffness and muscle activation were explored. Three of these combinations were selected based on parameter values from a previous modeling study (Robertson et al., 2014) and were as follows: (1) 100% *Stim* ($\omega_{spike} = 100$ Hz), 0% k_{MTU} ($k_{Exo} = 0$), (2) 80% *Stim* ($\omega_{spike} = 60$ Hz), 60% k_{MTU} ($k_{Exo} = 60\%\ k_{MTU}$), and (3) 60%*Stim* ($\omega_{spike} = 40$ Hz), 120% k_{MTU} ($k_{Exo} = 120\%\ k_{MTU}$) (Fig. 1B). The order of these trials was randomized to counteract fatigue effects.

Each set of dynamic contractions consisted of 10 stimulus pulse trains. The first five allowed the system to reach a steady state, and the last five were used in subsequent analysis (Fig. 1D and E). Each condition began with the mass sitting on a virtual 'table' which supported its weight until a target threshold force was reached. In previous experiments (Robertson and Sawicki, 2015), the table force threshold (F_{table}) was computed as follows:

$$F_{table} = (l_{out}/l_{in})Mg$$

where g is gravitational acceleration (9.8 m/s^2). In conditions with reduced activation, this constraint was relaxed. Table thresholds for $\omega_{stim} = 100$ Hz, 60 Hz, and 40 Hz conditions were 100%, 50%, and 25% of F_{table}, respectively.

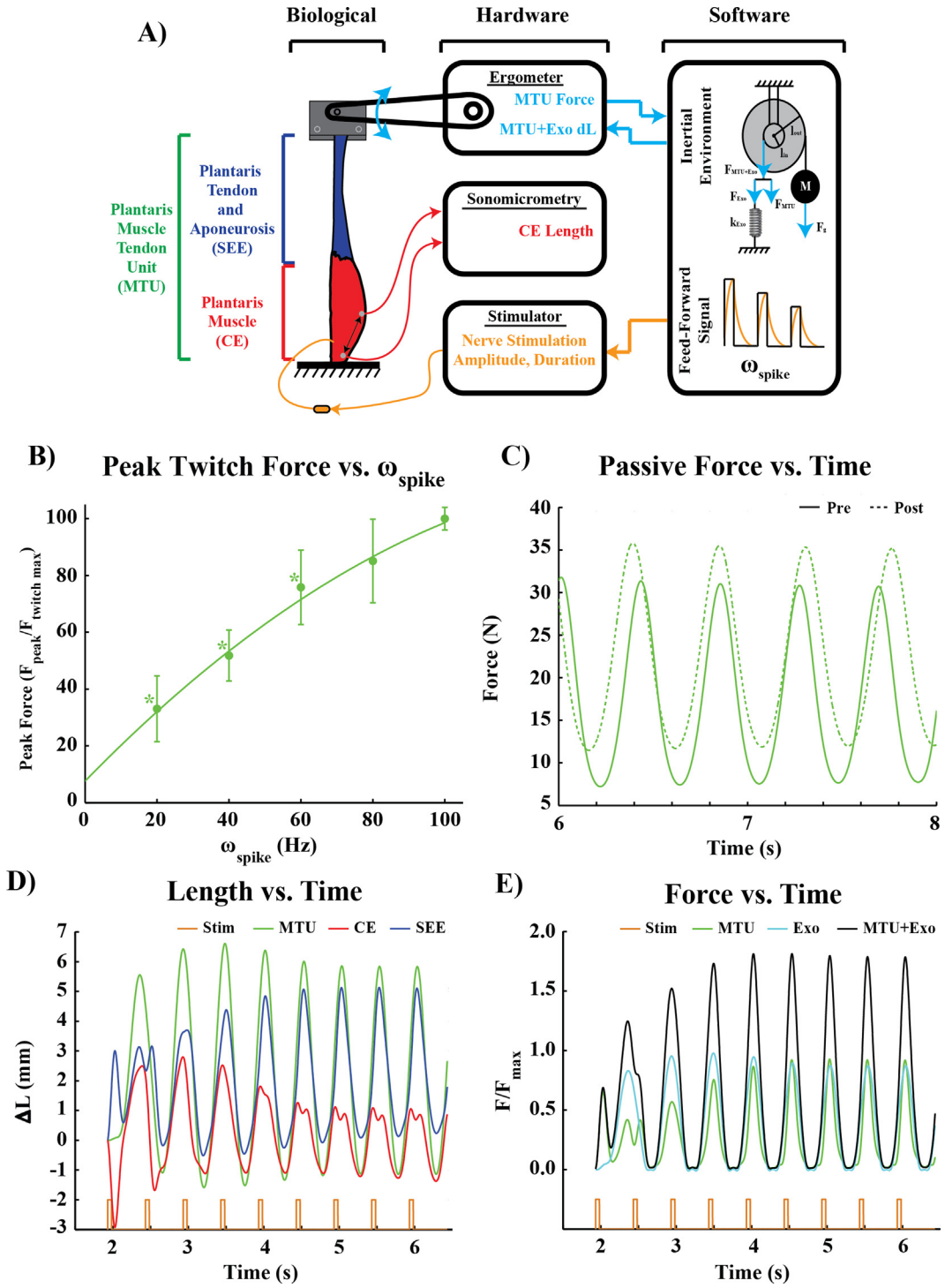

Fig. 1. (A) Schematic of experimental preparation. (B) Mean ± 1 SD normalized peak twitch force vs. stimulus frequency elicited using "pulsed" rate coding approaches (forces shown here are normalized to $\omega_{spike} = 100Hz$). A* indicates significant statistical differences in force from the 100 Hz condition. (C) Passive plucks performed pre- and post-experiment. Pre-experiment plucks were performed with inertial parameters known to be safe. Post-experiment plucks have values adjusted to drive estimated system ω_0 to 2.0 Hz. (D) Representative force (now normalized to F_{max}) and (E) length vs. time for the ($\omega_{stim} = 60$ Hz, $k_{Exo} = 60\%\ k_{MTU}$) condition. Note that the system rapidly stabilizes, and system-level (MTU + Exo) force is shared between biological MTU and simulated Exo.

Following all dynamic experimental conditions, a second set of 3 fixed-end contractions was performed. The average peak force was determined, and if the percentage of peak force achieved in the final set was >50% of that achieved initially, the experiment was considered a success (mean $\%Fatigue = 66.8 \pm 14.5\%$). Finally, a second passive pluck was performed to measure ω_0 with modified loading parameters selected to approximate $\omega_0 = 2$ Hz. This was performed last to avoid damaging biological tissue under increased loading conditions.

2.6. Experimental metrics

To insure consistent between-preparation comparisons, we normalized all absolute muscle (CE) length values to an estimated l_0, CE velocities to an estimated v_{max}, force data to a measured F_{max}, and metabolic and mechanical power metrics were scaled by CE mass (Robertson and Sawicki, 2015). Estimates of metabolic energy consumption were based on normalized muscle velocity and modeled

Table 1
Mean ± 1 SD values of measured and predicted physiological constants from all experimental subjects.

Physiological parameter	Mean ± STD
Initial ω_0	2.40 ± 0.11 Hz
Initial k_{MTU}	8559 ± 919 N/m
Adjusted l_{out}	23.6 ± 0.89
Adjusted M	0.095 ± 0.004 kg
Adjusted ω_0	2.25 ± 0.05 Hz
Final k_{MTU}	11,241 ± 681 N/m
F_{max}	42.00 ± 9.63 N
τ_{act}	0.074 ± 0.006 s
τ_{deact}	0.100 ± 0.02 s
l_0	14.57 ± 1.23 mm
v_{max}	−201 ± 17.03 mm/s
Muscle mass	5.52 ± 1.17 g
Animal mass	406.6 ± 42.6 g
Fatigue %	66.8 ± 14.5%

muscle activation level using estimates of activation and deactivation time constants (τ_{act} and τ_{deact}, respectively). Further details of calculations and assumptions used for experimental metrics can be found in Supplementary methods text.

2.7. Statistical analyses

For data that includes all subjects, outcomes over the last five stimulation cycles for each condition and preparation were averaged. These averages were then used as individual data points in statistical analysis to determine reported mean and standard error. We combined muscle activation and exoskeleton stiffness into a single descriptive independent variable called the "compensation index" (CI) computed as follows:

$$CI = (100 - \%Stim) + \%k_{MTU}$$

CI values for the (100% *Stim*, 0% k_{MTU}), (80% *Stim*, 60% k_{MTU}), and (60% *Stim*, 120% k_{MTU}) conditions were 0, 80, and 160, respectively. We performed one-way repeated measures ANOVA and regression fits for all metrics using the CI as the independent variable. ANOVA outcomes were considered significant for $p < 0.05$. Linear or nonlinear regression fits are presented depending on which was the best match to experimental data based on R^2 values. Regression fit equations, p values, and R^2 values for all reported data can be found in Table 2.

3. Results

3.1. Pulsed rate coding and activation/force modulation

Based on outcomes from this small study of fixed end contractions in the absence of series tendon, we determined that activation levels of 100%, 80%, and 60% could be reliably achieved for ω_{spike} values of 100 Hz, 60 Hz, and 40 Hz, respectively ($p < 0.0001$, $R^2 = 0.86$) (Fig. 1B, Table 1).

3.2. Work loop dynamics

For parameter combinations selected to mimic human neuromechanical response to an external device, MTU and/or MTU + Exo stiffness was generally constant and net work was ~0 in all conditions (Fig. 2Ai).

3.3. System dynamics vs. time

All experimental conditions shown here resulted in symmetric and alternating phases of lengthening/negative power and shortening/positive power (Fig. 2B–F). Within-subject standard devia-

Table 2
Table of regression fit order, equation, R^2, and p values for all reported metrics. A p value with bold text indicates a non-significant regression trend.

Metric	Fit order	Fit equation	R^2	p-value	Figure
MTU + Exo F_{peak}	2nd	$1.17 + 0.83CI - 0.32CI^2$	0.43	0.035	3A
MTU F_{peak}	1st	$1.18 - 0.35CI$	0.55	0.0015	3A
Exo F_{peak}	2nd	$0 + 1.15CI - 0.30CI^2$.	0.43	<0.0001	3A
%Phase F_{peak}	1st	$49.45 + 0.095CI$	0.002	**0.88**	3B
%Phase Stim Onset	2nd	$30.47 - 11.80CI + 13.77CI^2$	0.43	0.034	3B
k_{MTU}	1st	$0.96 - -0.004CI$	0.81	<0.0001	3C
$k_{MTU+Exo}$	1st	$0.98 + 0.0008CI$	0.19	**0.10**	3C
CE strain @ F_{peak}	2nd	$1.33 - 0.33CI + 0.15CI^2$	0.20	**0.085**	4A
CE velocity @ F_{peak}	2nd	$-0.003 - 0.01CI - 0.01CI^2$	0.06	**0.48**	4B
CE peak shortening velocity	2nd	$0.06 + 0.11CI - 0.03CI^2$	0.42	0.04	4C
MTU + Exo $\bar{P}^{+}_{mech}$	1st	$40.54 + 15.43CI$	0.27	0.046	5A
MTU + Exo $\bar{P}^{-}_{mech}$	1st	$43.51 - 10.93CI$	0.22	**0.079**	5A
MTU + Exo $\bar{P}^{net}_{mech}$	1st	$-2.96 + 4.50CI$	0.27	0.049	5A
MTU $\bar{P}^{+}_{mech}$	1st	$36.31 - 9.30CI$	0.39	0.013	5B
MTU $\bar{P}^{-}_{mech}$	1st	$-38.94 + 12.20CI$	0.55	0.0017	5B
MTU $\bar{P}^{net}_{mech}$	1st	$-2.62 + 2.90CI$	0.25	**0.06**	5B
CE $\bar{P}^{+}_{mech}$	1st	$12.47 - 1.17CI$	0.04	**0.46**	5C
CE $\bar{P}^{-}_{mech}$	1st	$-7.11 + 2.96CI$	0.33	0.025	5C
CE $\bar{P}^{net}_{mech}$	2nd	$5.37 + 0.018CI$	0.21	**0.35**	5C
SEE $\bar{P}^{+}_{mech}$	1st	$29.51 - 7.21CI$	0.31	0.031	5D
SEE $\bar{P}^{-}_{mech}$	1st	$-37.5CI + 8.33CI$	0.23	**0.076**	5D
SEE $\bar{P}^{net}_{mech}$	2nd	$-7.90 + 0.01CI$	0.3	**0.5**	5D
Exo $\bar{P}^{+}_{mech}$	2nd	$56.63CI - 19.92CI^2$	0.7	0.0008	5E
Exo $\bar{P}^{-}_{mech}$	2nd	$-5.57CI + 21.52CI^2$	0.74	0.0003	5E
Exo $\bar{P}^{net}_{mech}$	1st	$-0.34 + 1.63CI$	0.28	0.042	5E
$\%P^{+}_{mech}$ CE	2nd	$0.29 - 0.21CI + 0.08CI^2$	0.68	0.001	5F
$\%P^{+}_{mech}$ SEE	2nd	$0.71 - 0.56CI + 0.17CI^2$	0.81	<0.0001	5F
$\%P^{+}_{mech}$ Exo	2nd	$0.77CI - 0.25CI^2$	0.91	<0.0001	5F
$\bar{P}_{met}$	2nd	$82.21 + 3.13CI - 8.17CI^2$	0.25	**0.17**	6A
MTU + Exo ε_{app}	2nd	$0.46 + 0.51CI - 0.14CI^2$	0.46	0.024	6B
MTU ε_{app}	2nd	$0.46 - 0.17CI + 0.06CI^2$	0.20	**0.27**	6C
CE ε_{app}	2nd	$0.15 + 0.02CI - 0.01CI^2$	0.01	**0.96**	6D

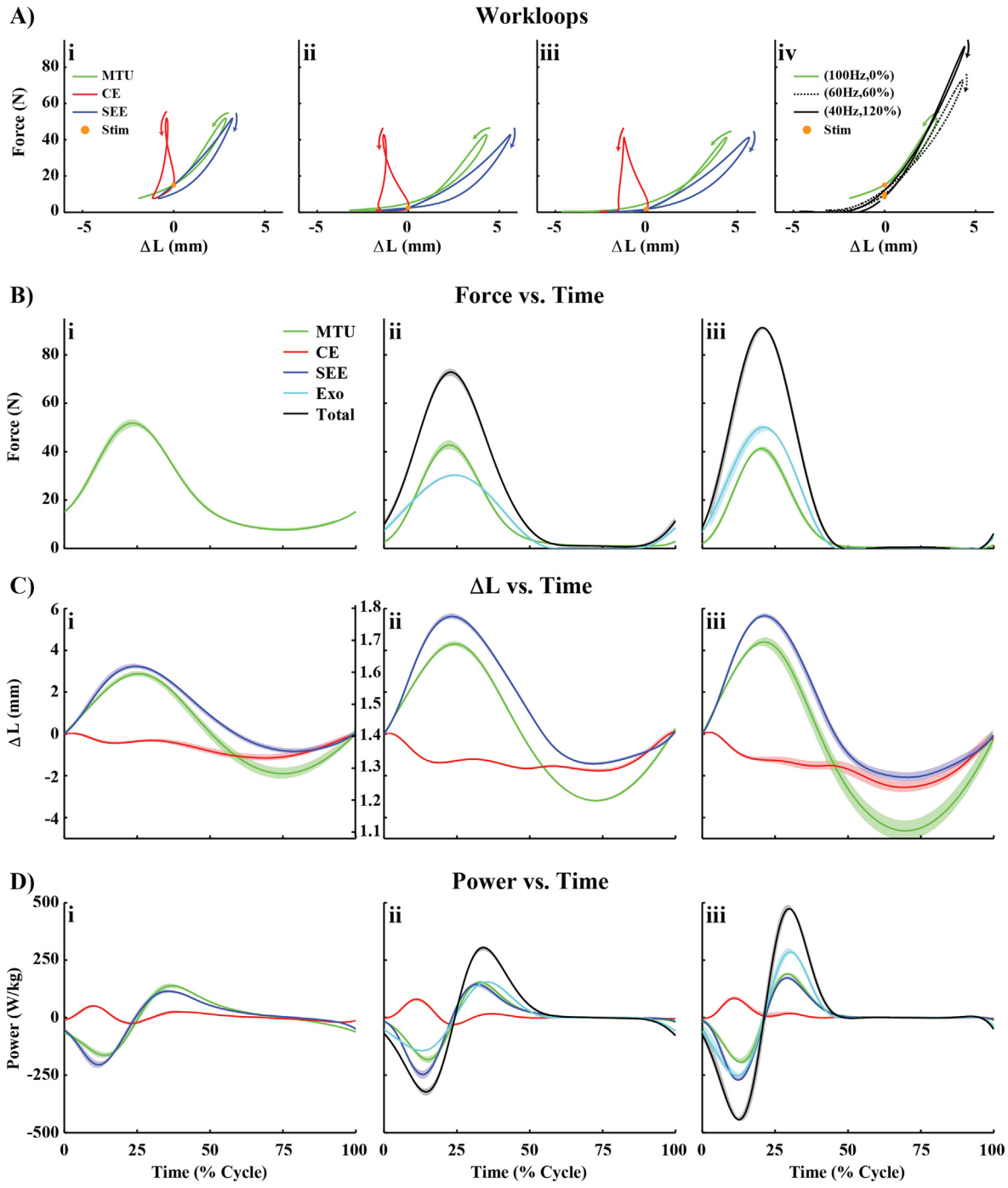

Fig. 2. (A) Representative mean work loops for biological components in the (i) (100 Hz, 0% k_{MTU}), (ii) (60 Hz, 60% k_{MTU}), and (iii) (40 Hz, 120% k_{MTU}) conditions, as well as (iv) MTU + Exo work loops for all three conditions. Note that while biological stiffness changes across conditions (i–iii), MTU + Exo (iv) does not. Representative time series data over 4 cycles ± 1 SE of (B) force, (C) length, and D) power versus time for the (i) (100 Hz, 0% k_{MTU}), (ii) (60 Hz, 60% k_{MTU}), and (iii) (40 Hz, 120% k_{MTU}) conditions. Note that biological excursions increase, force/power is shared between MTU and Exo components, and variation from cycle to cycle is generally small.

tions in force, length, and power vs. time were relatively low, and mechanical behavior was generally cyclic.

3.4. Peak force and phasing

For conditions meant to reflect human neuromechanical response to Exo assistance, MTU force decreased significantly ($p = 0.0015$, $R^2 = 0.55$) in agreement with **H1**, while Exo and MTU + Exo increased significantly ($p < 0.0001$, $R^2 = 0.86$ and $p = 0.035$, $R^2 = 0.43$, respectively) with increasing k_{Exo} and decreasing ω_{spike} (Fig. 3A, Table 2).

The phasing of peak force was consistent across all conditions, and occurred at almost exactly 50% of a cycle (Fig. 3B). The phasing of stimulation onset, however, varied significantly ($p = 0.034$, $R^2 = 0.43$) for conditions meant to be reflective of human behavior; and increased from ~30% in the (100 Hz, 0%k_{MTU}) condition, to ~50% in the (40 Hz, 120%k_{MTU}) condition (Fig. 3B, Table 2).

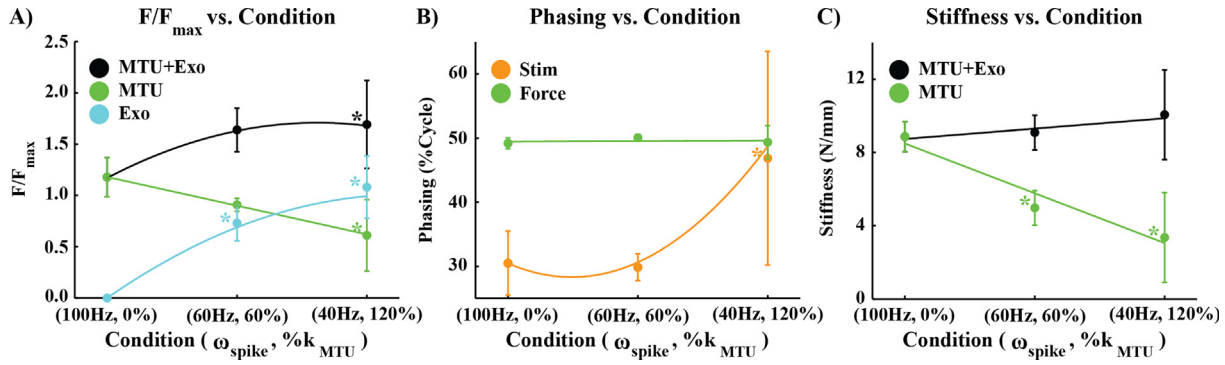

Fig. 3. Plots of (A) Peak force ± 1 SD for MTU + Exo, MTU, and Exo system components, (B) phasing of stimulation onset and peak force ± 1 SD relative to minimum MTU length within a given oscillation cycle, and (C) stiffness ± 1 SD of the MTU + Exo system and MTU only.

3.5. Muscle mechanical state

Significant trends were observed in muscle (CE) strain at peak force (Fig. 4A). No significant trends were observed in muscle (CE) velocity at the time of peak force (Fig. 3D, Table 2), but there were significant increases in peak shortening velocity within a stimulation cycle, in agreement with **H2** ($p = 0.04$, $R^2 = 0.42$) (Fig. 3E, Table 2).

3.6. Power output dynamics

For all conditions examined here, MTU + Exo $\bar{P}^{net}_{mech} \sim 0$, indicating mechanical behavior that was cyclic and steady (Fig. 5A). Significant increases in MTU + Exo $\bar{P}^{+}_{mech}$ ($p = 0.046$, $R^2 = 0.27$) (Fig. 5A) occurred concomitantly with significant decreases in MTU $\bar{P}^{+}_{mech}$ ($p = 0.013$, $R^2 = 0.39$) and $\bar{P}^{-}_{mech}$ ($p = 0.0017$, $R^2 = 0.55$) (Fig. 5B) (Table 2). We also observed significant decreases in the magnitude of CE $\bar{P}^{-}_{mech}$ ($p = 0.025$, $R^2 = 0.33$) (Fig. 5C), SEE $\bar{P}^{+}_{mech}$ ($p = 0.031$, $R^2 = 0.31$) (Fig. 5D), and, in agreement with **H3**, near constant CE $\bar{P}^{+}_{mech}$ in these conditions (Fig. 5D) (Table 2). This all coincided with significant increases in Exo P^{+}_{mech} ($p = 0.0008$, $R^2 = 0.70$) and Exo $\bar{P}^{-}_{mech}$ ($p = 0.0003$, $R^2 = 0.74$) (Fig. 5E, Table 2). When MTU power production was broken down into percent contribution from CE/SEE and Exo (where appropriate), there were significant decreases in both %CE ($p = 0.001$, $R^2 = 0.68$) and %SEE ($p < 0.0001$, $R^2 = 0.81$) $\bar{P}^{+}_{mech}$ occurring concomitantly with significant increases in %Exo $\bar{P}^{+}_{mech}$ ($p < 0.0001$, $R^2 = 0.91$) (Fig. 5F, Table 2).

3.7. MTU and MTU + Exo stiffness

Changes in MTU + Exo stiffness were non-significant across all conditions ($p = 0.10$, $R^2 = 0.19$), but MTU stiffness dropped significantly as exoskeleton stiffness increased ($p < 0.0001, R^2 = 0.81$) (Table 2, Fig. 3C), in agreement with **H4**.

3.8. Modeled metabolic cost and apparent efficiency, ε_{app}

For human-like combinations of ω_{spike} and k_{Exo} we observed decreased estimated metabolic demand (Fig. 6A), increased MTU + Exo ε_{app} (Fig. 5B), decreased MTU ε_{app} (Fig. 6C), and a relatively constant CE ε_{app} (Fig. 6D). The only significant trend was MTU + Exo ε_{app} ($p = 0.024$, $R^2 = 0.46$) (Table 2).

4. Discussion

Using previous modeling and experimental outcomes as a guide (Robertson et al., 2014; Robertson and Sawicki, 2014, 2015) we developed a benchtop biorobotic platform for directly observing muscle-level effects of parallel mechanical assistance from a passive elastic exoskeleton. We hypothesized and observed that combinations of reduced muscle (CE) activation (ω_{spike}) and increased exoskeleton (Exo) stiffness (k_{Exo}) exhibiting human-like behavior in modeling studies (Robertson et al., 2014) would result in **(H1)** reduced muscle-tendon unit (MTU) forces (Figs. 2 and 3A), **(H2)** increased muscle peak shortening velocities (Figs. 2 and 4B–C), **(H3)** constant muscle average positive mechanical power output, $\bar{P}^{+}_{mech}$ (Figs. 2 and 5C) and **(H4)** constant

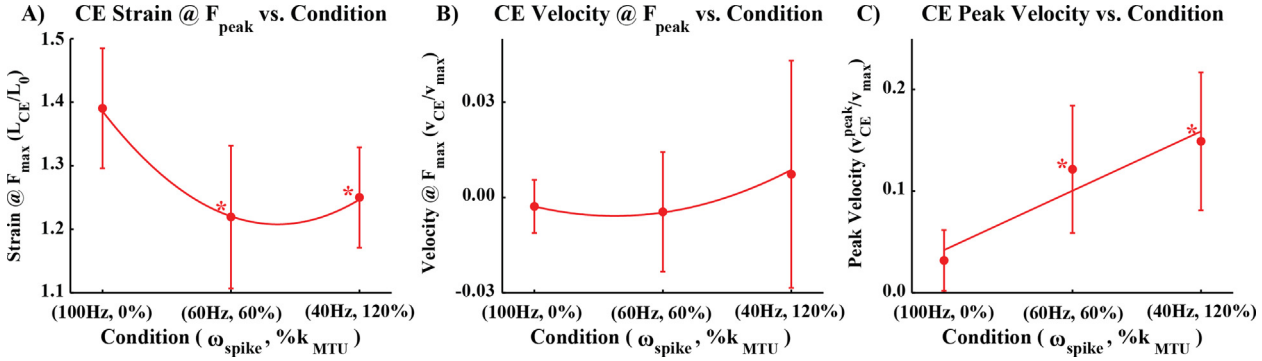

Fig. 4. Plots of (A) mean CE strain ± 1 SD and (B) mean CE velocity ± 1 SD at peak force, as well as (C) peak shortening velocity ± 1 SD within a stimulation cycle. Note that strains decrease and peak shortening velocities increase with added assistance/reduced activation, but velocity at F_{max} remains relatively constant.

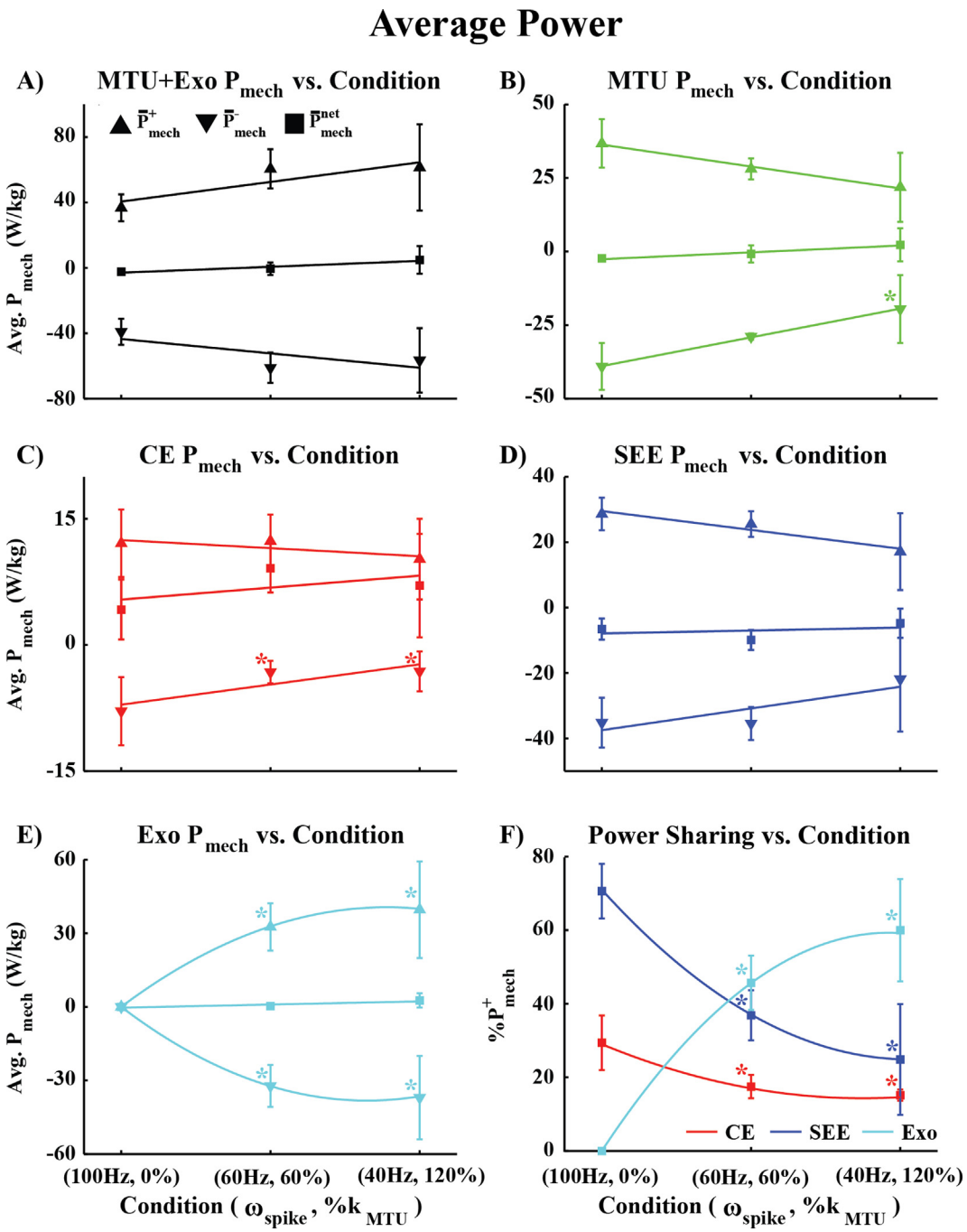

Fig. 5. Plots of mean ± 1 SD for positive (▲), negative (▼), and net (■) average power over a cycle of stimulation for (A) MTU + Exo, (B) MTU, (C) CE, (D) SEE, and (E) Exo; as well as (F) mean ± 1 SD of average positive power from the CE, SEE, and MTU for a cycle of stimulation. Note that only trends in power sharing vary significantly for all metrics presented.

system (MTU + Exo) stiffness ($k_{MTU+Exo}$) (Fig. 3C). These *in vitro* results aligned well with experimental outcomes from human experiments, establishing for the first time that neuromuscular adaptation to an assistive device can be replicated using a benchtop biorobotic platform.

Using our biorobotic testbed, we programmed an *in silico* parallel elastic exoskeleton (Exo) to deliver virtual forces that replaced a substantial portion of the biological MTU force observed in the unassisted condition (100 Hz, 0%k_{MTU}) (Fig. 3A). Peak MTU + Exo forces increased with decreasing ω_{stim} and increasing k_{Exo}, but the MTU experienced reduced loading (Fig. 3A). This, in turn, necessitated reduced tendon strains (*i.e.,* absolute lengths), and increased tendon excursions due to a shift in operating point onto the nonlinear (and more compliant) 'toe' region (Fig. 2aii-iii).

Reduced forces alone, however, did not guarantee the observed increases in muscle (CE) excursion that resulted in constant CE $\bar{P}^{+}_{mech}$. This behavior emerged due to decreased strain and increased compliance of the tendinous tissues (SEE) (Fig. 2Ai-iii, C) which increased CE shortening velocity (Fig. 4C) and reduced CE strain (Fig. 4A). Some combination of muscle activation dynamics, muscle force-length-velocity operating point, history dependent CE and SEE properties, and Exo dynamics drove this outcome; although it is not possible to identify how these factors contributed individually.

4.1. Exoskeletons impart performance benefits despite a 'de-tuned' neuromechanical system

Previous studies have demonstrated that, during bouncing gait, biological muscle-tendon (CE-SEE) interaction is 'tuned', with CEs generating high forces to remain strut-like and cycle energy in SEE's (Farris et al., 2013; Lichtwark and Wilson, 2005; Roberts and Azizi, 2011; Takeshita et al., 2006). By manipulating levels of CE activation (ω_{stim}) and exoskeleton (Exo) assistance k_{Exo} ($\%k_{MTU}$), we demonstrated that benefit can be derived from a 'de-tuned' biological system in the form of reduced biological force (Figs. 2A-B and 3A), CE strains (Fig. 4A), and estimated metabolic cost (Fig. 6A) as well as increased MTU + Exo apparent efficiency, ε_{app} (Fig. 6B). The only non-ideal outcome we found evidence for was decreased biological MTU ε_{app}, although trends were not significant (Fig. 6C). All of these observations are in line with those from human studies (Chang et al., 2008; Farris et al., 2013; Grabowski and Herr, 2009; Kao et al., 2010), except absolute CE strain, which increased in modeling studies (Robertson et al., 2014), and remained constant in human experiments of spring-loaded hopping (Farris et al., 2013).

4.2. Exoskeletons can modulate the frequency-phase coupling relationship that determines muscle-tendon (MTU) 'tuning'

Studies of human-exoskeleton interaction have demonstrated that some assistance can be metabolically advantageous, while too much can be detrimental (Collins et al., 2015; Grabowski and Herr, 2009). Others have shown that frequency of movement also influences where metabolic benefit is derived in spring-assisted hopping (Farris and Sawicki, 2012). Modeling studies have identified a terminal device stiffness, beyond which muscle activation must be increased rather than decreased to meet performance criteria (Robertson et al., 2014). While these studies collectively identify factors limiting benefits of lower-limb passive exoskeletons, they do not reveal the mechanisms underlying these emergent behaviors.

Our benchtop biorobotic approach provides some further insights into the mechanistic underpinnings of human-exoskeleton interaction. In a recent study probing neuromechanical control of resonant or 'tuned' MTU dynamics without exoskeleton assistance, we found that stimulating a biological MTU with feed-forward drive (ω_{drive}) matched to the system *passive* oscillation frequency (ω_0) resulted in highly tuned CE-SEE interactions. We also found that shifting ω_{drive} too far from ω_0 de-tuned the system, and significantly diminished energy storage/return in the SEE (Robertson and Sawicki, 2015). In the current study, we observed a comparable trend by altering ω_0 via increasing k_{Exo} with a constant ω_{drive} (Figs. 2, 3B and 5F). The effect, however, was the same. That is, a ω_{drive} misaligned to the system ω_0 resulted in de-tuned MTU mechanics.

Our benchtop studies suggest that there is a fundamental frequency-phase coupling relationship that ultimately determines whether muscle (CE) activation timing is suitable for elastic energy cycling in tendinous tissues (SEE). Furthermore, this frequency-phase coupling depends not only on passive stiffness of the involved biological tissues, but also the dynamics of the environment, both of which are influenced by the addition of exoskeleton assistance. These findings agree with previous studies of frequency-phase coupling during human bouncing (Merritt et al., 2012; Raburn et al., 2011). Merritt et al. showed that people prefer metabolically optimal movement frequencies during ankle-driven bouncing (Merritt et al., 2012). A follow-up study demonstrated that this preferred frequency of movement exhibited hallmarks of mechanical resonance

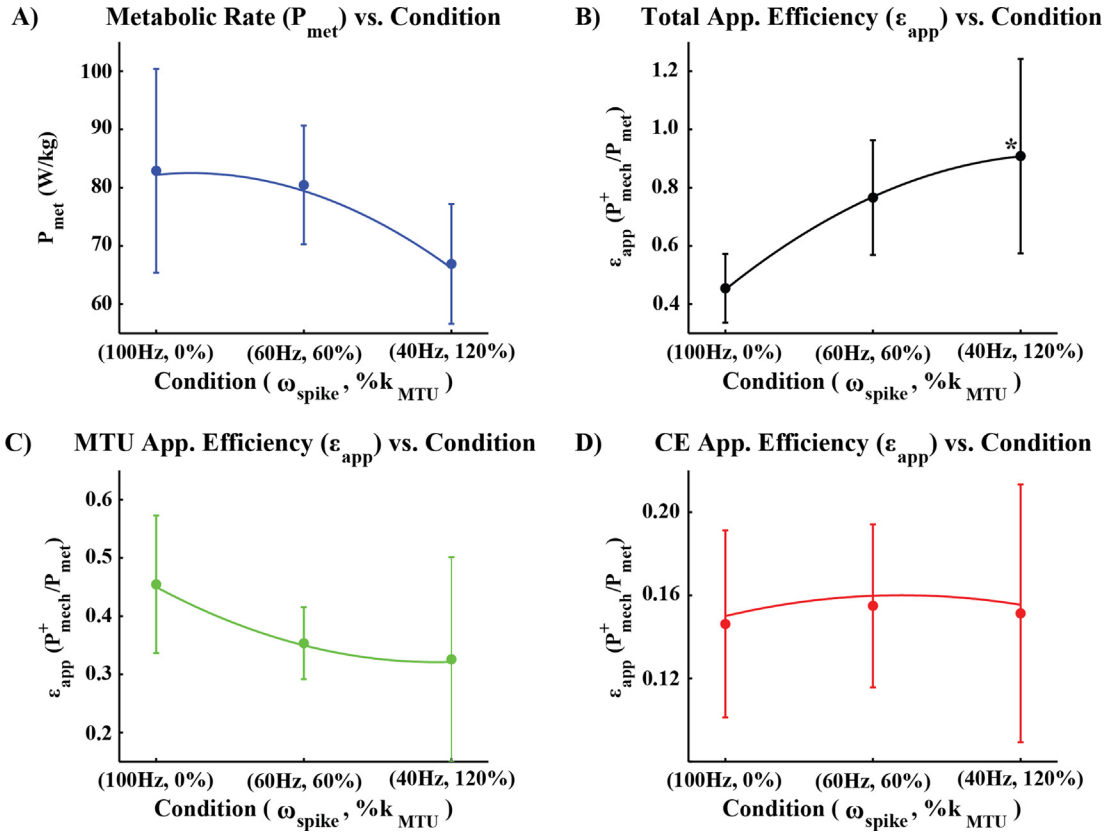

Fig. 6. Plots of mean ± 1 SD for (A) average metabolic rate, (B) total apparent efficiency, (C) MTU apparent efficiency, and (D) CE apparent efficiency. Note that only trends on overall system efficiency (i.e. MTU + Exo) are statistically significant.

(Raburn et al., 2011). Raburn et al. also observed that humans could identify new resonant frequencies after environment dynamics were altered by introducing stiffness or mass in parallel with the body; and that reflexes were necessary for rediscovering ω_0 (Raburn et al., 2011). This and previous studies collectively suggest that resonant movement frequencies for ankle-dominated tasks can be described simply by the relationship shown in Eq. (1), and that reflexive feedback is required for adaptation in novel mechanical environments (Merritt et al., 2012; Robertson and Sawicki, 2015).

4.3. Resonance as a guiding principle for 're-tuning' neuromechanical function

Conditions like spinal cord injury, stroke, and healthy aging result in observable gait pathologies that are accompanied by changes in material properties (*i.e.,* stiffness, k in Eq. (1)) of both muscle and tendon (Franz and Thelen, 2016; Maganaris et al., 2006; Magnusson et al., 2008; Zhao et al., 2009). It is also well documented that these clinical populations have altered neural reflex, which may limit their ability to identify new resonant movement frequencies due to structural changes in biological tissues. Findings from this study suggest that, especially for individuals with reduced ability to adapt novel coordination patterns via reflex modulation, elastic exoskeletons may offer a way to modify limb resonant frequency to match existing patterns of neural control and re-tune muscle-tendon interactions.

5. Future directions

We hope to test predictions from this study in humans during spring-assisted hopping across a range of stiffnesses applied at the ankle joint. If modeling and *in vitro* predictions are correct, there should be a 'goldilocks zone' in which assistance is not too stiff or too compliant, but just right. At the ideal exoskeleton stiffness, we would expect minimized muscle activity, minimized metabolic demand, constant system (*i.e.,* biological ankle + exoskeleton) stiffness, and constant average positive power in the major plantar flexors (*i.e.,* soleus, medial and lateral gastrocnemius). On the other hand, it is possible that at the highest exoskeleton stiffness settings, users could maintain their baseline neuromechanics and use the device to increase mechanical power output beyond normal physiological levels.

The benchtop biorobotic testbed we have demonstrated here is a powerful new tool that can be applied to explore the impact of environment dynamics on the mechanics and energetics of biological muscle-tendon unit (MTU) function. In future work, we hope to begin addressing how exoskeletons influence neural feedback during rhythmic movement by combining existing tools with instrumentation to record directly from 1a and 1b sensory afferents (*i.e.,* muscle spindles and golgi tendons) during simulated assisted and unassisted locomotion. This approach may give important insight into the neural mechanisms underlying adaptation to assistive devices.

Conflict of interest statement

We have no conflicts of interest to report.

Acknowledgements

We would like to thank funding sources, including grants from the UNC/NC State Rehabilitation Engineering Core (REC) and grant number 2011152 from the United States - Israel Binational Science Foundation awarded to GSS.

Appendix A. Supplementary material

Supplementary data associated with this article can be found, in the online version, at http://dx.doi.org/10.1016/j.jbiomech.2017.03.009.

References

Caputo, J.M., Collins, S.H., 2014. A universal ankle-foot prosthesis emulator for human locomotion experiments. J. Biomech. Eng. 136, 035002.
Chang, Y.H., Roiz, R.A., Auyang, A.G., 2008. Intralimb compensation strategy depends on the nature of joint perturbation in human hopping. J. Biomech. 41, 1832–1839.
Collins, S.H., Wiggin, M.B., Sawicki, G.S., 2015. Reducing the energy cost of human walking using an unpowered exoskeleton. Nature 522, 212–215.
Elliot, G., Sawicki, G.S., Marecki, A., Herr, H., 2013. The biomechanics and energetics of human running using an elastic knee exoskeleton. In: Proceedings of the IEEE International Conference on Rehabilitation Robotics (ICORR).
Farris, D.J., Robertson, B.D., Sawicki, G.S., 2013. Elastic ankle exoskeletons reduce soleus muscle force but not work in human hopping. J. Appl. Physiol. 115, 579–585.
Farris, D.J., Sawicki, G.S., 2012. Linking the mechanics and energetics of hopping with elastic ankle exoskeletons. J. Appl. Physiol.
Ferris, D.P., 2009. The exoskeletons are here. J. Neuroeng. Rehab. 6, 17.
Ferris, D.P., Lewis, C.L., 2009. Robotic lower limb exoskeletons using proportional myoelectric control. In: Proceedings of the 31st Annual International Conference of the IEEE Engineering and Medicine in Biology Society, Minneapolis, MN, USA.
Franz, J.R., Thelen, D.G., 2016. Imaging and simulation of Achilles tendon dynamics: implications for walking performance in the elderly. J. Biomech. 49, 1403–1410.
Grabowski, A.M., Herr, H.M., 2009. Leg exoskeleton reduces the metabolic cost of human hopping. J. Appl. Physiol. 107, 670–678.
Hasegawa, Y., Ogura, K., 2013. First report on passive exoskeleton for easy running: PEXER IV. In: Proceedings of the IEEE International Symposium on Micro-NanoMechatronics and Human Science, Nagoya, Japan.
Hocoma.
Josephson, R.K., 1999. Dissecting muscle power output. J. Exp. Biol. 202, 3369–3375.
Kao, P.C., Lewis, C.L., Ferris, D.P., 2010. Invariant ankle moment patterns when walking with and without a robotic ankle exoskeleton. J. Biomech. 43, 203–209.
Kawamoto, H., Lee, S., Kanbe, S., Sankai, Y., 2003. Power assist method for HAL-3 using EMG-based feedback controller. In: Proceedings of the IEEE International Conference on Systems, Man, and Cybernetics, Washington, D.C., USA.
Lichtwark, G.A., Wilson, A.M., 2005. In vivo mechanical properties of the human Achilles tendon during one-legged hopping. J. Exp. Biol. 208, 4715–4725.
Maganaris, C.N., Reeves, N.D., Rittweger, J., Sargeant, A.J., Jones, D.A., Gerrits, K., De Haan, A., 2006. Adaptive response of human tendon to paralysis. Muscle Nerve 33, 85–92.
Magnusson, S.P., Narici, M.V., Maganaris, C.N., Kjaer, M., 2008. Human tendon behaviour and adaptation, in vivo. J. Physiol. 586, 71–81.
Malcolm, P., Derave, W., Galle, S., De Clercq, D., 2013. A simple exoskeleton that assists plantarflexion can reduce the metabolic cost of human walking. Pub. Libr. Sci. One 8, e56137.
Merritt, K.J., Raburn, C.E., Dean, J.C., 2012. Adaptation of the preferred human bouncing pattern toward the metabolically optimal frequency. J. Neurophysiol. 107, 2244–2249.
Mooney, L.M., Rouse, E.J., Herr, H.M., 2014. Autonomous exoskeleton reduces metabolic cost of human walking during load carriage. J. Neuroeng. Rehab. 11, 80.
Panizzolo, F.A., Galiana, I., Asbeck, A.T., Siviy, C., Schmidt, K., Holt, K.G., Walsh, C.J., 2016. A biologically-inspired multi-joint soft exosuit that can reduce the energy cost of loaded walking. J. Neuroeng. Rehab. 13, 43.
Pennycuick, C.J., 1964. Response of fast muscle fibres to series of impulses. J. Exp. Biol. 41, 291–298.
Raburn, C.E., Merritt, K.J., Dean, J.C., 2011. Preferred movement patterns during a simple bouncing task. J. Exp. Biol. 214, 3768–3774.
Rack, P.M., Westbury, D.R., 1969. The effects of length and stimulus rate on tension in the isometric cat soleus muscle. J. Physiol. 204, 443–460.
Roberts, T.J., Azizi, E., 2011. Flexible mechanisms: the diverse roles of biological springs in vertebrate movement. J. Exp. Biol. 214, 353–361.
Robertson, B.D., Farris, D.J., Sawicki, G.S., 2014. More is not always better: modeling the effects of elastic exoskeleton compliance on underlying ankle muscle-tendon dynamics. Bioinspiration Biomimetics 9, 046018.
Robertson, B.D., Sawicki, G.S., 2014. Exploiting elasticity: modeling the influence of neural control on mechanics and energetics of ankle muscle-tendons during human hopping. J. Theor. Biol. 353, 121–132.
Robertson, B.D., Sawicki, G.S., 2015. Unconstrained muscle-tendon workloops indicate resonance tuning as a mechanism for elastic limb behavior during terrestrial locomotion. Proc. Natl. Acad. Sci. U.S.A.
Sawicki, G.S., Khan, N.S., 2016. A simple model to estimate plantarflexor muscle-tendon mechanics and energetics during walking with elastic ankle exoskeletons. IEEE Trans. Biomed. Eng. 63, 914–923.
Stevens, E.D., 1996. The pattern of stimulation influences the amount of oscillatory work done by frog muscle. J. Physiol. 494 (Pt 1), 279–285.

Takeshita, D., Shibayama, A., Muraoka, T., Muramatsu, T., Nagano, A., Fukunaga, T., Fukashiro, S., 2006. Resonance in the human medial gastrocnemius muscle during cyclic ankle bending exercise. J. Appl. Physiol. 101, 111–118.

Wehner, M., Quinlivan, B., Aubin, P.M., Martinez-Villalpando, E., Baumann, M., Stirling, L., Holt, K., Wood, R., Walsh, C., 2013. A lightweight soft exosuit for gait assistance. In: Proceedings of the IEEE International Conference on Robotics and Automation (ICRA), Karlsruhe, Germany.

Wiggin, M.B., Collins, S.H., Sawicki, G.S., 2011. An exoskeleton using controlled energy storage and release to aid ankle propulsion. In: Proceedings of the 12th International IEEE Conference on Rehabilitation Robotics, Zurich, Switzerland.

Zhao, H., Ren, Y., Wu, Y.N., Liu, S.Q., Zhang, L.Q., 2009. Ultrasonic evaluations of Achilles tendon mechanical properties poststroke. J. Appl. Physiol. 106, 843–849.

Zoss, A.B., Kazerooni, H., Chu, A., 2006. Biomechanical design of the Berkley lower extremity exoskeleton (BLEEX). IEEE/ASME Trans. Mechatron. 11, 128–138.